**UNIVERSAL WISER**
PUBLISHER

Review

# Organic Solar Cells with Nanofibers in the Active Layer Obtained by Coaxial Electrospinning

**Yngrid Synara de Sena Silva, Maria de Fatima Vieira Marques**[*]

Institute of Macromolecules Professor Eloisa Mano/Federal University of Rio de Janeiro, Av. Horácio Macedo, 2.030, Bloco J, Cidade Universitária, CEP 21941-598-Rio de Janeiro-RJ-Brazil
E-mail: fmarques@ima.ufrj.br

**Abstract:** The high demand for energy and the intensification of climate change have led to the need to improve renewable energy sources, such as solar energy. Organic bulk heterojunction (BHJ) cells using conjugated polymers as the electron donor in the active layer are an alternative because they are easy processability, flexible, have the absorption spectrum corresponding to the structure of the polymer, and can be synthesized in an endless variety of chemical structures. One of the limiting factors for large-scale applications was the relatively low conversion of solar energy into electricity, but this has been practically overcome recently, as efficiencies of around 20% have been achieved for small-area devices and around 16% for larger devices, approaching conventional silicon cells. The device's stability remains the most restraining factor, as it has to last at least ten years in sun and weather exposure. This review presents works that improve the efficiency of photovoltaic devices by addressing the development of materials used in the active layer (semiconductor polymers and acceptor materials). Additionally, the use of nanofibers in the active layer obtained by the electrospinning technique is discussed. The nanofiber quality parameters (solute properties, solution properties, processing conditions, and environmental conditions) are discussed, including coaxial electrospinning.

*Keywords*: BHJ solar cell, electrospinning, conductive polymer, electron acceptor material

## 1. Introduction

Technological revolutions in the last fifty years have required greater energy consumption in different sectors of society. The use of non-renewable energy sources for large-scale energy production is leading to the depletion of fossil material resources at a rapid pace and resulting in higher greenhouse gas emissions [1]. Therefore, renewable energies (biomass, wind, hydroelectric, tidal, geothermal, and solar) are candidates for reducing the emission of these gases and attenuating global warming and its consequences [2].

The implementation of solar energy can be justified because the Earth's atmosphere has a high solar incidence (about $1.75 \times 10^{17}$ W per day) [3], which will result in a good direct conversion of solar energy into electricity [4]. Photovoltaic solar cells can be divided into four generations. The first two generations have their development and operation guided by inorganic semiconductors (silicon and cadmium telluride). These materials result in a high cost due to the difficulty of processing and obtaining the final device [5].

Third-generation solar cells have the advantages of ease of processing, optical transparency, lightness, low

production cost and the possibility of obtaining flexible cells. These photovoltaic devices can be mainly divided into perovskite solar cells (PSCs), organic photovoltaic cells (OPVs), and dye-sensitized solar cells (DSSCs) [6]. In the present work, the focus will be on the study of OPVs, where the active layer comprises the mixture of electron donor/acceptor, which have an advantage over other third-generation photovoltaic cells in the possibility of controlling polymeric structures to increase the spectrum of absorption of sunlight, either through the use of new polymer structures as donors, and the development of new acceptors. Furthermore, applying two donor polymers and one acceptor, or vice-versa, in the same layer (ternary cell) or establishing a connection between two active layers through an intermediate layer (tandem cell) could capture a higher frequency range of the solar spectrum, greatly increasing the efficiency in energy conversion [7].

Among the different types of OPV, this work will emphasize solar cells with an active layer that presents a morphology of bulk heterojunction (BHJ), addressing the main groups of donor polymers and acceptor materials of this cell. In addition, it will address a bibliographic survey emphasizing research carried out using electrospinning for manufacturing nanofibers to be incorporated into this active layer to relate the parameters of the technique with photovoltaic performance.

Figure 1 shows the graph resulting from the bibliometric study. For this purpose, the ScienceDirect database was used to search for the following keywords: Third generation solar cells. It is possible to observe a growth trend in the number of publications in the area. Still, few works include electrospinning materials for this application.
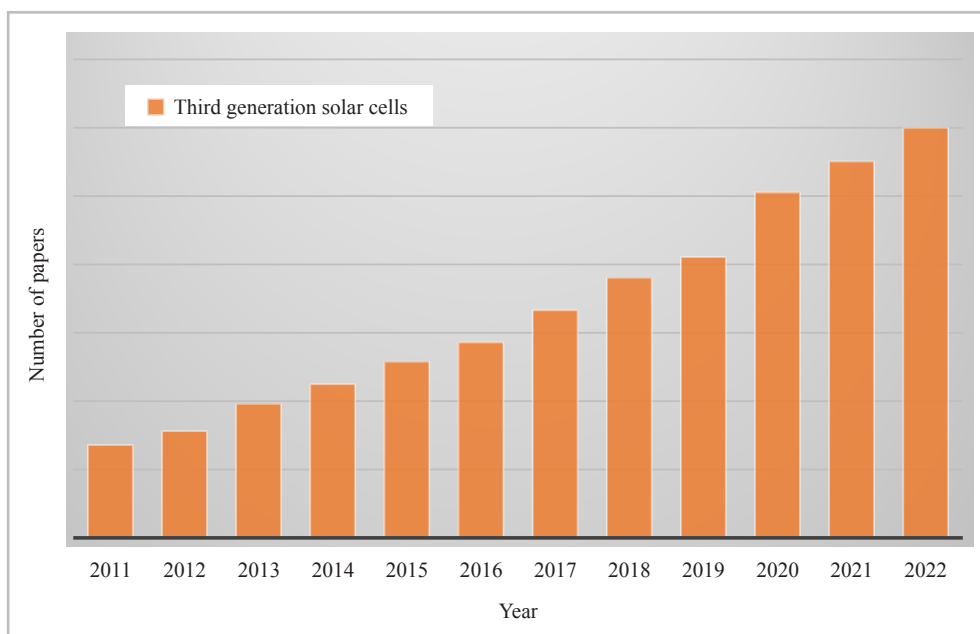


**Figure 1.** Bibliometric study of third-generation solar cells and BHJ

# 2. Organic photovoltaics
## 2.1 *Bulk heterojunction solar cell (BHJ)*

The conventional BHJ solar cell has as a characteristic to be a multilayer device, among which we can mention: i) substrate; ii) transparent layer of indium and tin oxide (ITO) as a hole collection electrode; iii) carrier layer of holes; iv) active layer; v) electron carrier layer (Ca or LiF); and vi) metallic electrode (Al) [8].

The active layer is the one in which the process of light absorption and generation of charges occurs, which are formed by the presence of at least two materials: an electron donor based on a conjugated polymer as type-p semiconductor, and an acceptor material, type-n semiconductor (mostly a fullerene derivative), to form the p-n junction

[9]. In the BHJ structure, this layer has as characteristic the nanodomains of the acceptor material interpenetrating the donor polymer, as shown in Figure 2. Conjugated polymers have a delocalized π-electron system resulting from the alternate single and double bonds. The acceptor can be derived from fullerenes or other materials with high electron affinity [10].
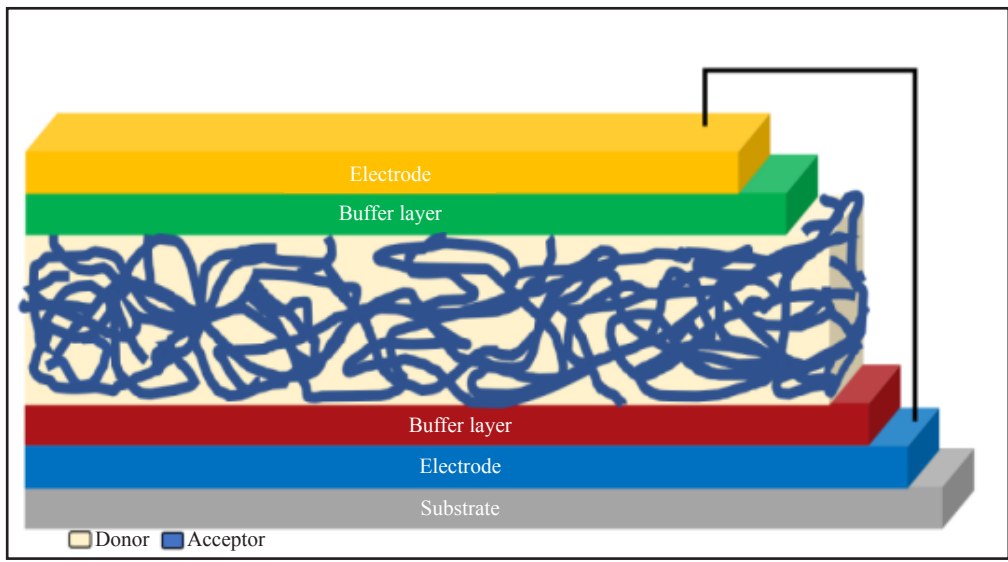


**Figure 2.** Representation of a BHJ cell and the mechanism of conversion of photons to electrons into OPV
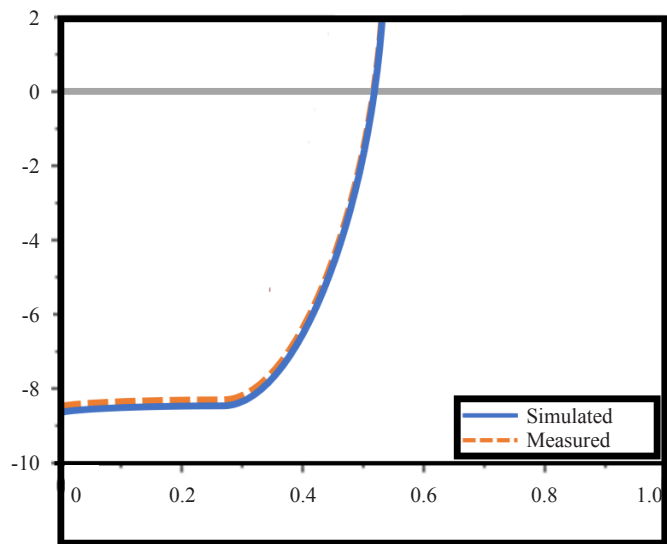
## 2.2 *Photovoltaic parameters*



**Figure 3.** A comparison between the simulated J-V characteristics and measurements of a device with configuration ITO/PEDOT:PSS/Donor:acceptor/Al

The parameters of a photovoltaic cell are taken from a voltage-current density curve (J-V), as shown in Figure 3.

The parameters obtained in this curve are short circuit current density ($J_{sc}$), open circuit voltage ($V_{oc}$), fill factor (FF), and power conversion efficiency (PCE) [11].

The short circuit current density ($J_{sc}$) is related to the current density generated without applying an external voltage (when the voltage is zero), proportional to the number of photons absorbed by the active layer. The value depends on the intensity and absorption range of the materials of the active layer [12]. $V_{oc}$ is the voltage compensating for the current flow through the external circuit; it is the maximum voltage measured in the illuminated device when the current is nullified. It is related to the miscibility of the materials that make up the solar cell and is also dependent on the highest occupied molecular orbital (HOMO) energy level of the donor polymer and the lowest unoccupied molecular orbital (LUMO) value of the acceptor material [13]. The FF is characterized as the quadrature of the current-voltage density curve (J-V) and is related to the possibility of photogenerated carriers being extracted from a photovoltaic device. On the other hand, PCE is related to converting incident photons into electricity. The calculation is based on multiplying FF, $J_{sc}$, and $V_{oc}$ values divided by the incident power, which is standardized [14] at 1,000 $W/m^2$.

## 2.3 *Operation of a BHJ solar cell*

The functioning of a BHJ-type solar cell can be subdivided into some steps: i) Light absorption and generation of excitons, ii) Diffusion of excitons and dissociation of charges, iii) Charge transport, and iv) Collection of charge carriers in electrodes [15].

In the first stage, the process begins with the light being incident on the transparent electrode, the photon is absorbed, and the electron excitation in the conductive polymer occurs from HOMO to the LUMO orbitals. An exciton (electron-hole pair) is formed in this process, with binding energy typically between 0.1 to 1.4 eV. At this stage, the active layer should absorb maximum incident light to achieve a maximum efficiency value. This absorption is limited to the thickness of the active layer (about 100 nm) due to the low charge mobility of polymer semiconductors. However, the optimization of absorption is inversely proportional to the bandgap of the polymer; that is, the smaller the difference between HOMO and LUMO, the greater the electron flow [16].

After the formation of the excitons, these need to diffuse in the active layer and form the charge carriers (electron and hole). The diffusion of the formed charges is limited to a length of up to 20 nm due to its short service life and the possibility of recombining the electron-hole pair, annihilating the exciton. Therefore, the efficient diffusion length is when the formed exciton generates charge carriers; that is, the exciton achieves enough energy to transpose the Coulomb binding energy. The source for making such energy transposition comes from the electric field created by the electrostatic forces at the interface of the acceptor and donor materials. Consequently, free electrons are attracted to the LUMO of the acceptor material, and the formed hole is attracted to the HOMO of the donor polymer [12, 16].

With the excitons dissociated and the formation of charge carriers, they are transported to their respective electrodes. This transport occurs basically due to the difference in the Fermi level of the electrodes. The main limitation is the recombination of charge carriers before reaching their anode or cathode. Materials with low mobility have the electron and hole attracted by electrostatic force, which favors recombination and, consequently, the loss of efficiency of the device [17].

The collection of charges in the respective electrodes completes the steps of light absorption for photocurrent generation. The maximization of this stage is characteristic of the reduction of the potential barrier in the photoactive layer and the interface of the electrodes [18]. Usually, buffer layers are added between the BHJ layer and the anode (HTL, hole transport layer) and another before the cathode (ETL, electrons transport layer) to decrease the exciton annihilation.

Another way to discuss the operation of a conventionally architectural BHJ solar cell is through the energy levels of each component, as shown in Figure 4. For the proper functioning of the BHJ cell, the energy levels present in the active layer must allow the formed electron to be able to transfer to the LUMO (or conduction band in inorganic semiconductors) of the ETL layer until reaching the cathode, as they have lower energy values. In turn, the hole formed in the active layer will go to HTL and then to the anode if the HOMO (or valence band) has higher energy values. More recently, new conjugated polymer structures have been developed, further increasing the PCE of the devices. The PTQ-10, PM-6 and D18 polymers [19] stand out (Figure 5).
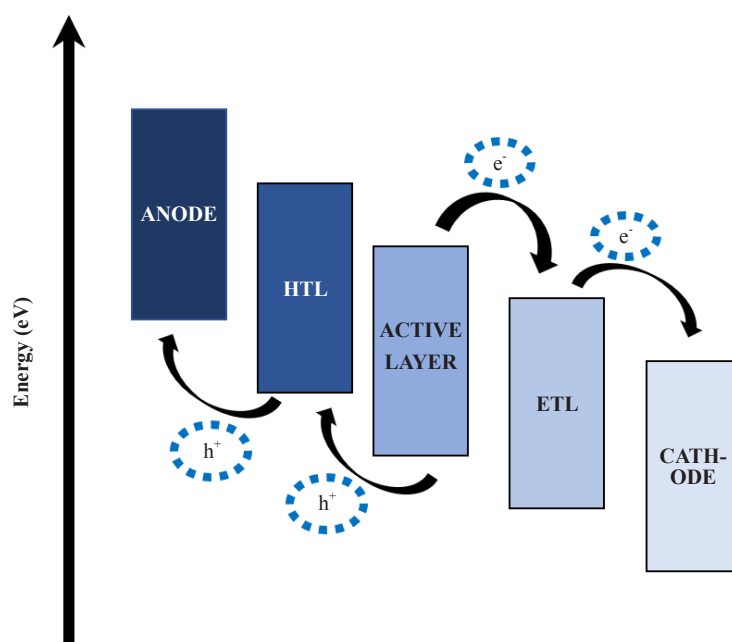
**Figure 4.** BHJ energy band diagram with conventional architecture

### 2.3.1 *Optical studies*

The first polymer to be used as a donor material was poly(2-methoxy-5-(2'-ethyl-hexyloxy)-1,4-phenylene vinylene) (MEH-PPV) (Figure 5a), in which the acceptor material used was the 6,6-phenyl $C_{61}$ butyric acid methyl ester ($PC_{61}BM$) and the efficiency in the cell energy conversion was 2.9%. This polymer is limited by low charge mobility and a narrow absorption spectrum [17, 20].

A class of materials widely used as a donor polymer involves polythiophenes, and the first most used was poly(3-hexylthiophene) (P3HT) (Figure 5b). This polymer has high charge mobility, good solubility, and excellent crystallinity [15, 21]. Polyfluorenes (PFs) (Figure 5c) are part of another class of widely used polymers, which have as characteristics good performance in charge transport, ease of forming an anisotropic crystalline structure, and a rigid planar structure [22]. However, devices with PFs as active layers have a low current due to the high bandgap value [23]. Developing donor polymers with lower bandgaps is paramount to minimize such consequences. Among the polymers with lower bandgap values, those with a structure based on benzothiophene, such as PTB7 and PTB7-Th* (Figure 5(d)) [24]. These polymers enable a lower bandgap as a result of the quinoid structure; a higher value of $V_{oc}$ due to the presence of fluoride atoms, which decrease the value of HOMO; a solubility favored by the side chains, and a good hole mobility thanks to the planar conjugated structure [25]. More recently, new conjugated polymer structures have been developed as electron donors, further increasing the PCE of the devices. The PTQ-10, PM-6 and D18 polymers stand out (Figure 5).
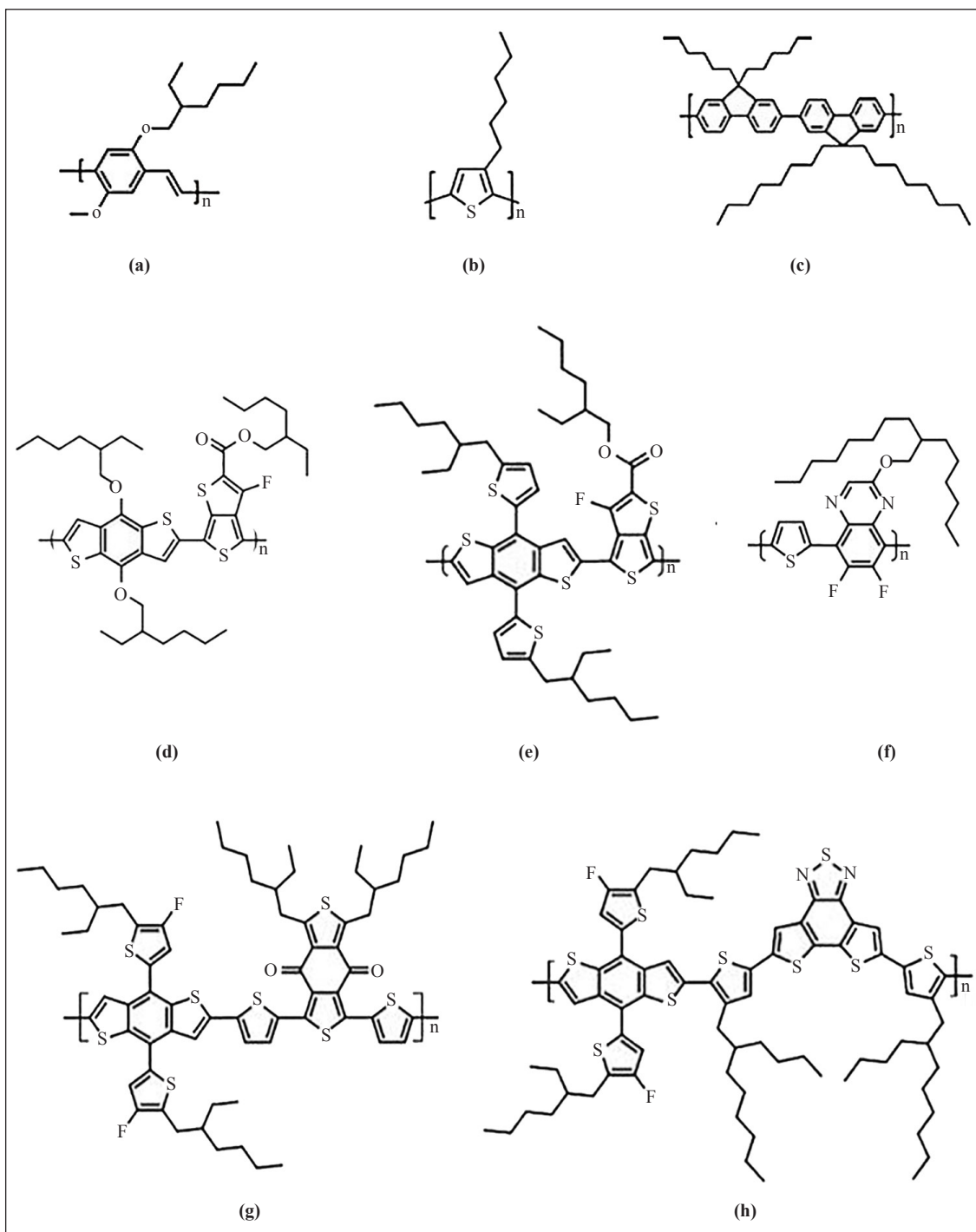
**Figure 5.** Structures of donor polymers: a) MEH-PPV; b) P3HT; c) PF; d) PTB7; (e) PTB7-Th; (f) PTQ-10; (g) PM-6; (h) D18

### 2.3.2 Electron acceptor materials
### 2.3.2.1 Phenyl-C$_x$-butyric acid methyl ester (PC$_x$BM)

Since the first work with BHJ cells was reported by Yu and collaborators [26], the most used acceptor material is fullerene and its derivatives [27]. Among the reasons for such use are the ability to accept the electron easily; good electron mobility; nanoscale morphology with a size similar to the diffusion length of an exciton, and the presence of

delocalized LUMOs, which provide charge percolation [28]. In addition, the ability to support the transport of electrons in three dimensions, different from most molecules or polymers, can help the properties of fullerene derivatives [29]. The most commonly used fullerene derivatives are $PC_{61}BM$ and $PC_{71}BM$. However, the disadvantages of fullerene and its derivatives consist of limited electronic affinities; weak absorption in the visible region (380 to 700 nm) and the near-infrared (NIR) region, between 800 and 2,500 nm; thermal and photochemical instability and the need for time-consuming purification, which contributes to high costs, although the absorption of $PC_{71}BM$ derivatives is stronger [30]. It led to the development of new electron acceptors to replace fullerenes.

### 2.3.2.2 *Non-fullerene acceptors (NFA)*

Another possibility of type-n semiconductors different from fullerenes is named NFAs. These p-conjugated organic materials have the advantage of great variability in chemical structure and electronic affinity; in some cases, they can be more easily synthesized than fullerene acceptors [29]. NFAs can be divided into two main groups based on their chemical structure, represented in Figure 6. In the first group, the chemical structure must have the electron push-pull effect. Intramolecular charge transfer (ICT) generally occurs in push-pull molecular systems containing dipolar organic chromophores, an electron donor (D) and an electron acceptor (A). Most exhibit small bandgaps and relatively strong dipoles, contributing to efficient ICT. In contrast, the second group comprises fused aromatic diimides or perylene diimides (PDI) [30-31].
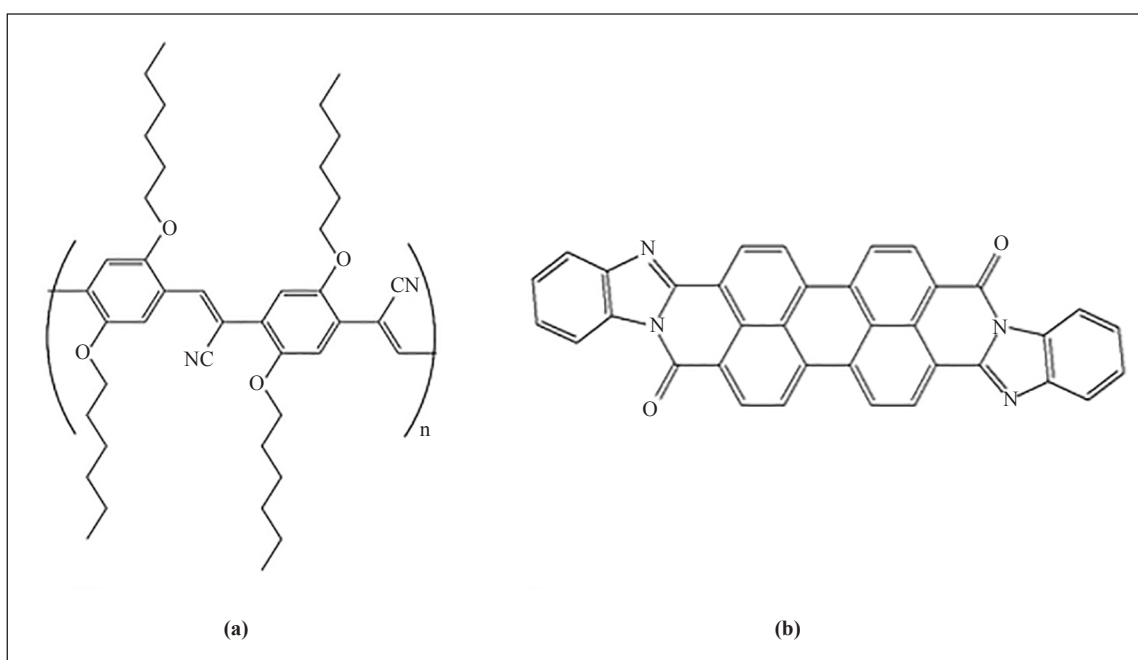


**Figure 6.** Representation of NFAs: a) poly(p-phenylene vinylene) (a) derivative of PPV (electron push-pulling effects). (b) N,N9-di(1-nonadecyl) perylene-3,4,9,10- bis(dicarboximide) (PDI-C9)(PDI)

These two groups have similarities. The first is the presence of highly electronegative elements such as oxygen (in the carbonyl group) and nitrogen (in the nitrile species, or even forming a hetero-aromatic group) in the constitution of the main conjugated structure [32]. The presence of these atoms allows the polymer chain to receive and stabilize the electron. The second characteristic of NFA groups is the presence of well-delocalized $\pi$ electrons in the entire main chain. These favor the transport of electrons in the active layer with a low energy cost, preventing them from being trapped and suffering recombination [33].

However, the disadvantages of NFAs are due to their anisotropic crystalline structure and planar orientation. The

first results in a decrease in transport and an ineffective extraction of electrons. The second affects the energy and dynamics of charge separation [34].

The first acceptor used in the research with the tunneling effect was cyanine phenylene (CN-PPV), which has a cyan linked to the ethylene group, allowing the relocation of electrons along the structure. Even so, the device obtained with this acceptor and with the electron donor poly(2-methoxy-5-(2'-ethyl-hexiloxy)-1,4-phenylene vinylene) (MEH-PPV) presented a PCE of only 0.04% [35]. Another widely used compound is ITIC, 3,9-bis(2-methylene-(3-(1,1-dicyanomethylene)-indanone))-5,5,11,11-tetrakis(4-hexylphenyl)-dithieno[2,3-d:2',3'-d']-s-indaceno[1,2-b:5,6-b'] dithiophene, and its derivatives, which have as characteristics a low bandgap, strong ability to accept electrons and many p-p interactions due to the molecular geometry [28, 35]. The ITIC compound can be modified by incorporating electron-deficient (such as fluoride) or electron-rich (such as methyl or methoxy) groups through a covalent bond with the aromatic nucleus. The incorporation of fluoride creates a compound called IT-4F that causes an increase in the absorption spectrum, making it wider and with greater intensity, resulting in a device efficiency of 13.1% [36]. On the other hand, the methyl group incorporation in ITIC decreases LUMO and increases $V_{oc}$, and the device reached a PCE of 12.1% [30, 37].

The second group of NFAs has as characteristic the presence of polyimide derivatives (PDI) with other nuclei p conjugated [38]. The main advantages are the electronic affinity comparable to fullerene's, strong absorption, intermolecular p interaction, which favors high electron mobility ($\mu_e$), and high thermal and oxidative stability [39]. However, when using a simple monomeric imide, the value of PCE was relatively low. For example, a study by Shin et al. [40] revealed PCE in a device with an active layer of P3HT:N, N-di (nonadecan-10-yl) with a value of 0.18%. In these cells, one of the reasons for the loss of efficiency was the deactivation of the excitons due to the formation of excimer (excited dimer).

Therefore, the synthesis of polymers presenting in their structure units of perylene diimide (PDI) conjugated with dithieno thiophene (DTT) [41] was initiated. These polymers have as characteristic the presence of electron-rich conjugated bridges, which provides a donor character, resulting in a PCE of 1.1% [42]. Subsequently, copolymers were synthesized with other aromatic systems, such as carbazoles and thiophenes. With the incorporation of the thiophenes, it was possible to obtain a BHJ cell with a PCE of 4.4% [43]. Another structural modification was the insertion of vinyl bonds that increase the planarity of the chain, the p-p interactions, and the charge transport. In Guo et al. [44], it was observed that the presence of vinyl bonds increased electron mobility, and the device resulted in a PCE of 7.57%.

There is still a great limitation in the values of photovoltaic parameters in BHJ solar cells based on the materials currently used as donors and acceptors. One attempt is to improve the transport and transfer of charges in these solar cells, increasing the crystallinity of the active layer [45]. The increase in crystallinity produces continuous pathways between donors/acceptors, improves charge transport, and causes less recombination between electrons and holes by increasing the p-p stacking of polymer chains [46].

Some efficient approaches to increasing crystallinity are the realization of annealing (thermal annealing) and annealing by solvent. Thermal annealing becomes virtually unfeasible for large-scale manufacturing using the roll-to-roll method [47]. In addition, thermal annealing cannot be employed when the device has a flexible substrate since these materials, usually poly(ethylene terephthalate), has a vitreous transition temperature of about 60 °C [48].

With the need to control the morphology of the active layers of BHJ devices and increase the crystallinity of conjugated polymers, promoting increased electrical properties and solar cell efficiency [49], electrospinning is a good alternative. It is a well-established, direct, and high-yield technique for manufacturing nanofibers with varying diameters, from nanometers to micrometers. The fibers obtained can provide a flexible and continuous spatial structure, facilitating light absorption. In addition, the promotion of crystallinity occurs due to the stretching of the polymer chain during electrospinning [50]. The mixture between donor polymers and electron acceptors is expected to be more intimate, and the molecules will be more oriented, facilitating charge transfer and decreasing exciton annihilation.

# 3. Electrospinning technic

The first electrostatic effects were observed in the water in the 1700s. But it was not until 1897 that Rayleigh invented electrospinning. Fibers were obtained by electrospinning in 1930 by Formhals, in which fibers were formed without dies, thus resulting in a patent for the process, the apparatus, and the obtaining of fibers of numerous polymers

employing an electrostatic method [51].

In 1968, Taylor studied the drop shape of a polymeric solution ejected under a strong electric field called the Taylor cone. In addition, other factors that affect fiber stability were studied: electric field, solution flow, and other experimental conditions. Until 1990, electrospinning was not widely used, as the fiber formation rate is about 30 m/min, while fusion wiring has a fiber formation rate of 1,500-2,000 m/min. The interest in using electrospinning is related to its ability to form nanofibers [52].

Electrospinning involves manufacturing nanofibers from polymeric solutions under a high electric field at atmospheric pressure and room temperature. The electrospinning equipment is shown in Figure 7. It has three main components: power supply (high voltage), needle (spinneret), and collector (electrode). The high-power supply voltage generates electrical charges in the polymer solution. These charges are accumulated until they overcome the surface tension present in the solution and form Taylor's cone. A jet from this cone is ejected, which runs through the entire electric field to the collector with opposite charges and converts into solid fibers by evaporation of the solvent [53-54].



**Figure 7.** Conventional electrospinning equipment

The process of evolution of the droplet shape during electrospinning is shown in Figure 8. In this process, the drop of polymeric solution coming out of the needle goes through some modifications in its shape. The first image (on the left and above) is Taylor's cone, in which the positively charged solution at the tip of the needle becomes a conical shape. Then the tip of Taylor's cone becomes sharper, and a charged jet is ejected into the collector. Finally, this cone recovers its hemispherical shape, a jet of charged liquid that undergoes stretching and thinning stably from the drop of polymeric solution [55-56].

However, the jet formed from the needle hole begins to curl and suffer a series of electrically induced instabilities that influence the nanofibers' morphology [57-58]. Three instabilities are identified; Rayleigh jet instability, axisymmetric instability, and whiplash. The first instability is characterized by a domain of surface tension and is suppressed by high electric fields. Axisymmetric instability is responsible for modulating the jet radius to ball-like structures. Whipping instability involves electrical competition between the free charges and the electric field, independent of surface tension. In addition, this instability is induced by two mechanisms: the repulsion of surface charges and the depolarization of the charges due to the interaction with the electric field [59-60]. The various electrospinning parameters also affect nanofiber quality, as will be addressed next.
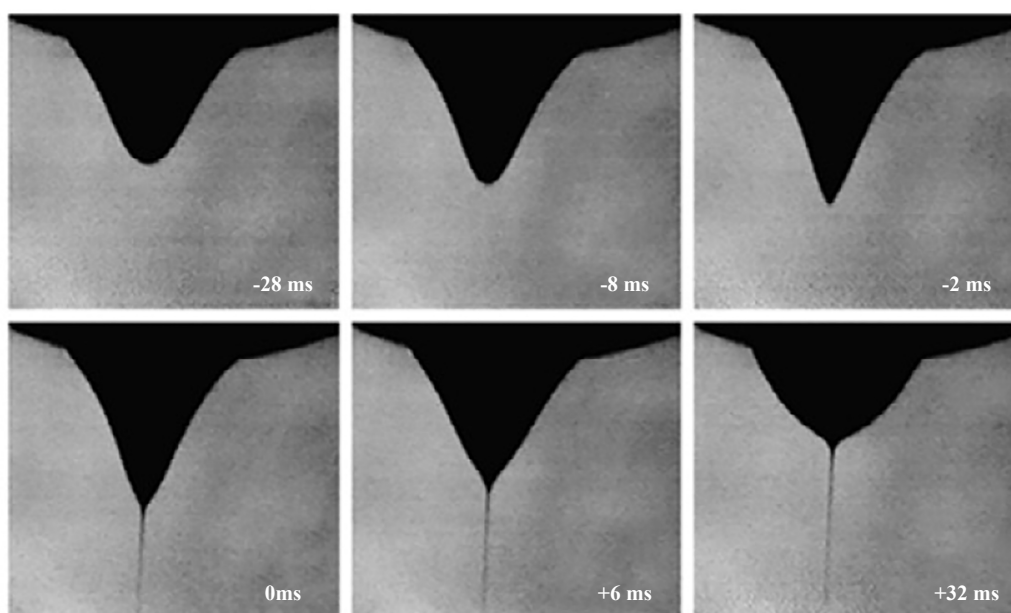
**Figure 8.** Process of the evolution of the shape of a solution drop under the electric field registered every 2 ms. Reprinted with permission from [16]

## 3.1 *Electrospinning parameters*

Several parameters can determine the surface's morphology and electrolyte nanofibers' dimensions and orientations in electrospinning. These parameters are (a) solute properties, including molar mass; (b) properties of the solution, like conductivity, concentration, and viscosity; (c) processing parameters, such as the distance between needle and collector, the electrical potential applied; the flow of the solution and the dimensions of the needle hole; (d) environmental conditions, including humidity and temperature [51-56, 60].

The property of the solute (the value of the molar mass of the polymer) is a determining factor for the diameter of the nanofiber. A study conducted by Rwei et al. [60] with PVA solutions, whose molar masses have different values, with the largest of 80,000 g/mol ($PVA_1$) and the smaller one of 16,000 g/mol ($PVA_2$), were electrospun in order to obtain an interval in which the concentrations allowed the formation of nanofibers with larger diameters and the absence of granules. For $PVA_1$, it was observed that no nanofiber was formed at a concentration of less than 6% by mass because the polymer was too diluted to allow the molecules to be tangled. On the other hand, for $PVA_2$, the limiting value for the absence of nanofibers was a concentration of 14% by mass. However, the maximum concentration of the solutions was 14% by mass for $PVA_1$ and 24% by mass for $PVA_2$. The main factor determining the maximum concentration was the value of the formed electric field, which became insufficient in the face of the viscosity of the electrospinning solution.

The first property of the solution to be discussed is conductivity, an important parameter in the electrospinning process that affects the charge density of the solution [61]. As the conductivity of the solution increases, more charges can be transported, resulting in a greater stretch of the polymer jet under a high electric field and a decrease in the diameter of the nanofiber [62]. Levitt et al. [63] studied the influence of the conductivity of a PAN solution relating them to the concentrations of 10%, 12%, and 15% by mass in the DMF solvent. They found that the effects of conductivity and concentration compete with each other. In addition, the viscosity effect of the solution on the diameter of the nanofiber dominated the effects of the conductivity of the solution, causing an increase in the diameter of the nanofiber with the increase of the polymer concentration.

The other properties of the solution (concentration and viscosity) are the two main factors in determining polymer chain entanglement [63-64]. The ability of polymer molecules to tangle is an effective indicator for forming nanofibers during electrospinning. For entanglement, the polymer chains must be valued above a critical concentration ($C^*$) [65]. This concentration can be discussed by taking into account the polymeric molar mass ($M_w$) and the effective volume ($R_g^3$)

occupied by the polymer chain in the solution [66], as in Equation 1.

$$C^* = \frac{3M_W}{4\pi R_g^3 N_A}.$$

(1)

$N_A$ is the Avogadro constant.

Another way to discuss the influence of the critical concentration of a polymeric solution is through Figure 9. Three different systems can be observed, with concentrations of polymeric solutions below, equal to, and above the critical concentration [67]. At low concentrations (diluted systems), polymer chains do not overlap (Figure 9a), and individual polymer chains govern the viscoelasticity of the solution. With the increase of polymer concentration, reaching the critical value, the polymer chains begin to overlap and tangle (Figure 9b). On the other hand, at values higher than the critical concentration, the entanglement of the chain increases rapidly (Figure 9c), which generates an abrupt increase in the viscoelasticity of the solution [58, 68].



|     |     |     |
| --- | --- | --- |
| (a) | (b) | (c) |
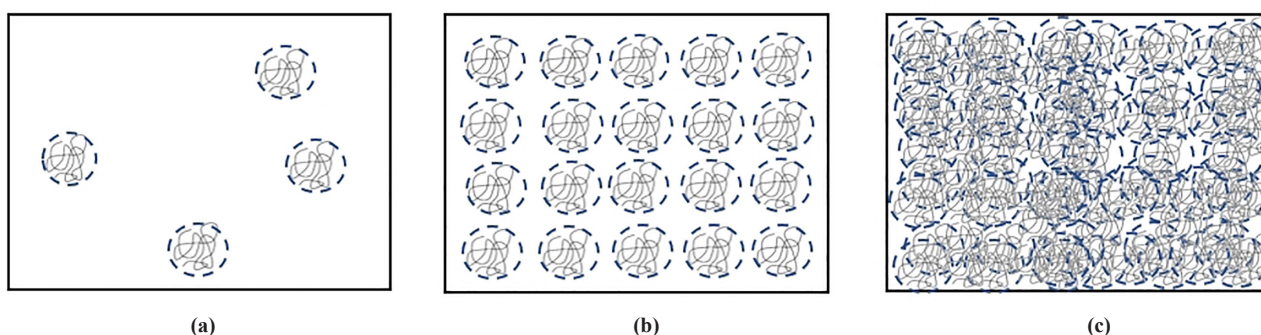
**Figure 9.** Effect on the viscosity of the solution and the feasibility of electrospinning: (a) polymer chains in dilute solution; (b) chain entanglement in the polymer at critical concentration; (c) chain entanglement in concentrated solutions

The viscosity of the polymer solution, its concentration, and the ability to electrospinning is related to the slope of a graph log of the viscosity of the polymeric solution x log of the polymeric solution concentration (Figure 10) [68]. As can be noticed, it shows two inclinations (~1.4 and ~3.4) related to non-electrospinning ability and electrospinning systems, respectively. At ~1.4 inclination, the system cannot electrospun as the solution is below the critical concentration, resulting in insufficient entanglement and the formation of beaded fibers due to the surface tension of the liquid (Rayleigh instability). However, for electrospinning to be stable, a concentration of the polymer solution higher than the critical concentration c*, i.e., the inclination of the graph is ~3.4. Interactions between several polymer chains govern this system's rheological behavior [58].

In Bakar and collaborators [69], the concentration of polyacrylonitrile (PAN) in a dimethylformamide (DMF) solution significantly affected the morphology of non-woven manufacturing. A weak non-tissue of polymeric material with cone morphology was obtained in solutions with low concentrations (6% and 8%). On the other hand, the solutions of higher concentrations (15% and 17%) resulted in dense cones that were difficult to form nanofibers. The concentration with the best formation of nanofibers was 10% of PAN in DMF.

Al-Dhahebi and collaborators [70] conducted a study using different concentrations (14%, 16%, and 18%) of (poly vinylidene fluoride) (PVDF) in acetone and DMF. The study found through scanning electron microscopy (SEM) that increasing the polymeric concentration of PVDF improved the morphological structure of nanofibers due to improved molecular chain entanglement, allowing the elongation of fibers during the electrospinning process. In addition, with a higher polymer concentration, granules were absent (Figure 11).
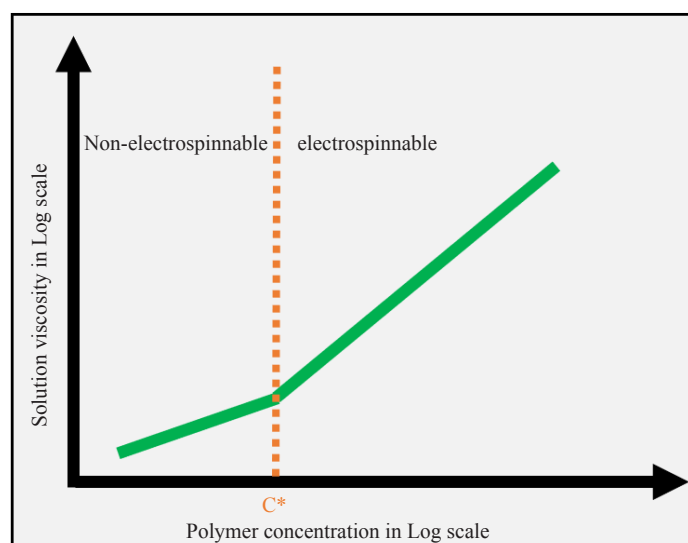
**Figure 10.** Solution viscosity graph vs. polymer concentration
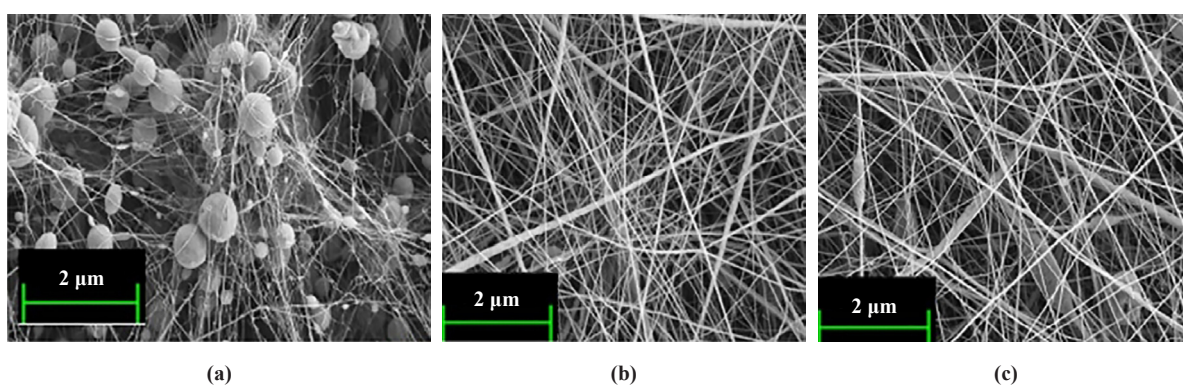


**Figure 11.** SEM image in PVDF concentration at 14% (a), 16% (b), and 18% (c), respectively. Reprinted with permission from [70]

Another study of the influence of the concentration of a polymeric solution in the electrospinning process, but this time, containing polyvinylpyrrolidone (PVP) in ethanol solvent with $TiO_2$ nanofiller, was carried out with the following polymer mass relations in solution: 7%, 8%, 9% and 10% by mass. The images of the SEM analysis are presented. In Figure 12a, it was observed that many elliptical granules were formed in the electrolyte material at the concentration of 7% by mass of PVP. With the increase of PVP concentration to 8%, the granule structures obtained were reduced (Figure 12b). At the concentration of 9% PVP (Figure 12c), uniform and smooth nanofibers were observed without any granule formation. However, at a concentration of 10% by mass of PVP, the nanofiber jet caused instability, and the nanofibers were formed with an irregular diameter (Figure 12d). The variation in the mass amount of PVP affects the viscosity of the precursor solution and the entanglement of the polymer chain in a solution. A low viscosity results in low viscoelasticity and a low electrostatic force, which is not suitable for the processing of electrospinning. However, viscoelasticity can be improved by increasing the concentration of the polymer, leading to the formation of uniform layers and smooth nanofibers without any granule structures. However, by increasing the polymeric concentration and viscosity of the solution, instability is created in the nanofiber jet, resulting in high electrostatic forces during electrospinning [71].
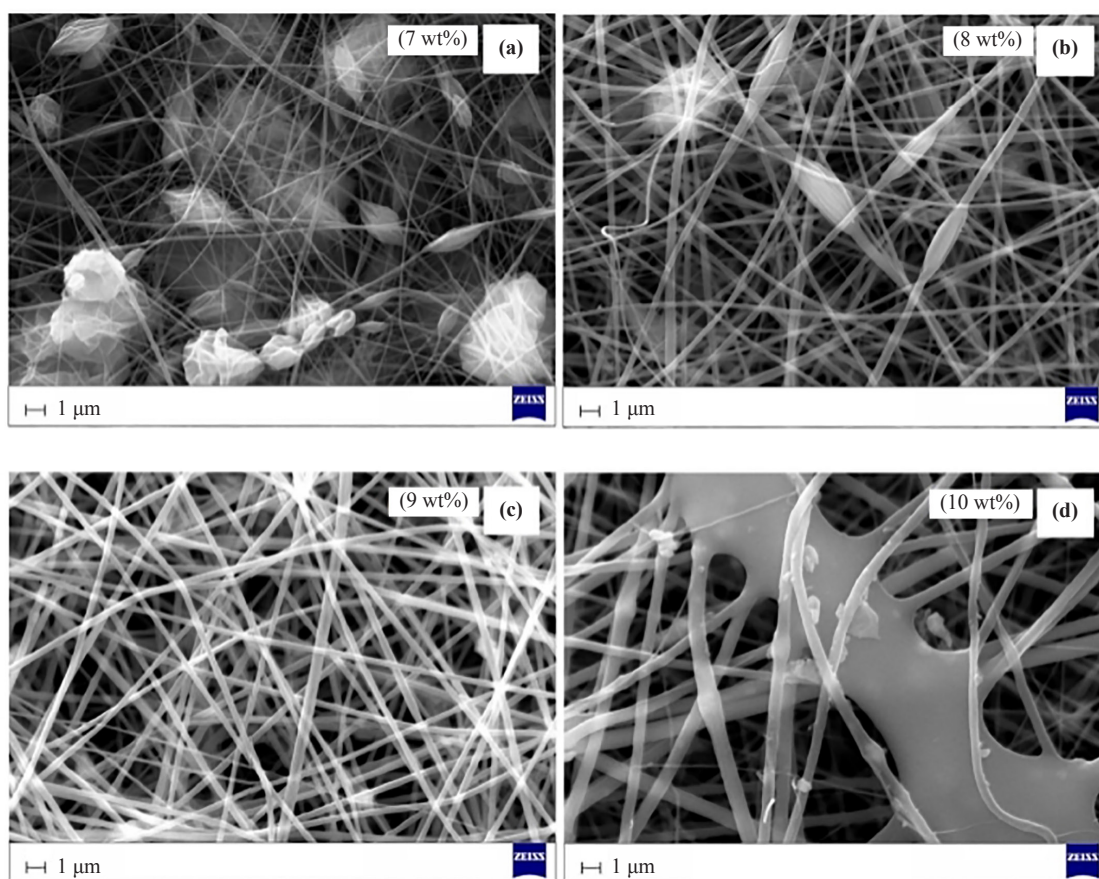
**Figure 12.** SEM images of TiO$_2$ nanofibers spun at different concentrations of PVP (a) 7 wt%, (b) 8 wt%, (c) 9 wt%, and (d) 10 wt%. Reprinted with permission from [71]

Another study on the consequence of increasing the concentration of polymer solution affecting the viscosity of the solution, surface tension, and consequently the diameters of the nanofibers was carried out by Lee et al. [72]. The authors studied the electrospinning of a poly(L-lactide) (PLLA) solution in chloroform/2,2,2-trifluoroethanol (TFE) (60:40) with concentrations of 1.5%, 2.75%, and 3.5%. The diameters of the nanofibers obtained were 248 ± 29 nm, 545 ± 78 nm, and 872 ± 97 nm, respectively. At very low concentrations, surface tension inhibits the formation of continuous fibers. On the other hand, at very high concentrations, the high viscosity hinders the flow of the solution through the tip of the needle.

The influence of processing parameters may favor or attenuate the presence of granules or even influence the diameter and morphology of nanofiber [73]. The formation of granules is favored because, in certain jet regions, there is an attempt to minimize surface-free energy. Depending on the distance between the needle tip and the collector, the polymeric solution coming out of the needle may or may not separate before reaching the collector. The short distance value favors fibers of larger diameters, which tend to attenuate the formation of granules due to the force of surface tension. The jet may not fully lengthen, and fiber solidification may not occur when it reaches the collector. However, if the distance is long enough, the fiber will stretch and elongate as much as possible before solidifying. In the collector, it will form a solid fiber on the surface [55, 57, 62, 73].

A work that exemplifies the influence of the distance between the needle and the collector was developed by Gade et al. [74]. It was observed that a solution of PVDF in acetone/DMF (1:1), when electrospun with different distances between collector and needle (12 cm, 15 cm, 18 cm, and 22 cm), recorded a decrease in the diameter of the nanofibers (316 nm, 266 nm, 242 nm, 224 nm, respectively). Another factor analyzed was how this experimental parameter affected the morphology of nanofibers through the content of the crystalline β phase of PVDF. The higher value of the

distance between the needle and collector allowed greater elongation of the fibers, resulting in an increase in β phase content from 88.98% (at a distance of 12 cm) to 91.92% at a distance of 22 cm.

Another important processing parameter is the applied voltage because, together with the parameter of the distance between the needle tip and the collector, there is the determination of the electric field [65]. In addition, the high voltage introduces the necessary charges into the electrospinning solution, assisting the process. For several polymers, higher voltage increases electrostatic repulsive forces in the ejected jet, decreases fiber diameter and causes rapid solvent evaporation [67].

The tension applied to the polymeric solution during electrospinning influences the diameter and morphology of the nanofiber. The diameter of the nanofiber can be decreased with the increase of the electric field [57, 74]. An example is a work in which PVDF nanofibers obtained from a solution whose solvent is DMF: acetone(1:1) suffered a 67% reduction in the nanofiber diameter with the increase of the voltage values from 21 KV to 30 KV. In this same study, the FTIR technique showed how different values of applied stresses influence the crystalline morphology of PVDF (crystalline β phase content) in electrospun nanofibers. The PVDF crystal in the β phase is the main responsible for the piezoelectric effect of the material. When mechanical stress is applied, this phase provides a better formation of electrical charges in a material. In addition, the PVDF in the β phase has characteristic absorption bands at 840 $cm^{-1}$ and 1275 $cm^{-1}$. The authors found that the crystal content of the β phase decreased from 91.9% in 21 kV to 89% in 30 kV. The justification for this is that, with the increase in the applied stresses, the number of potential ions in the jet ejected becomes very high, which creates an increase in jet instability and leads to a decrease in the electroactive energy for the formation of the crystal in the β phase [74].
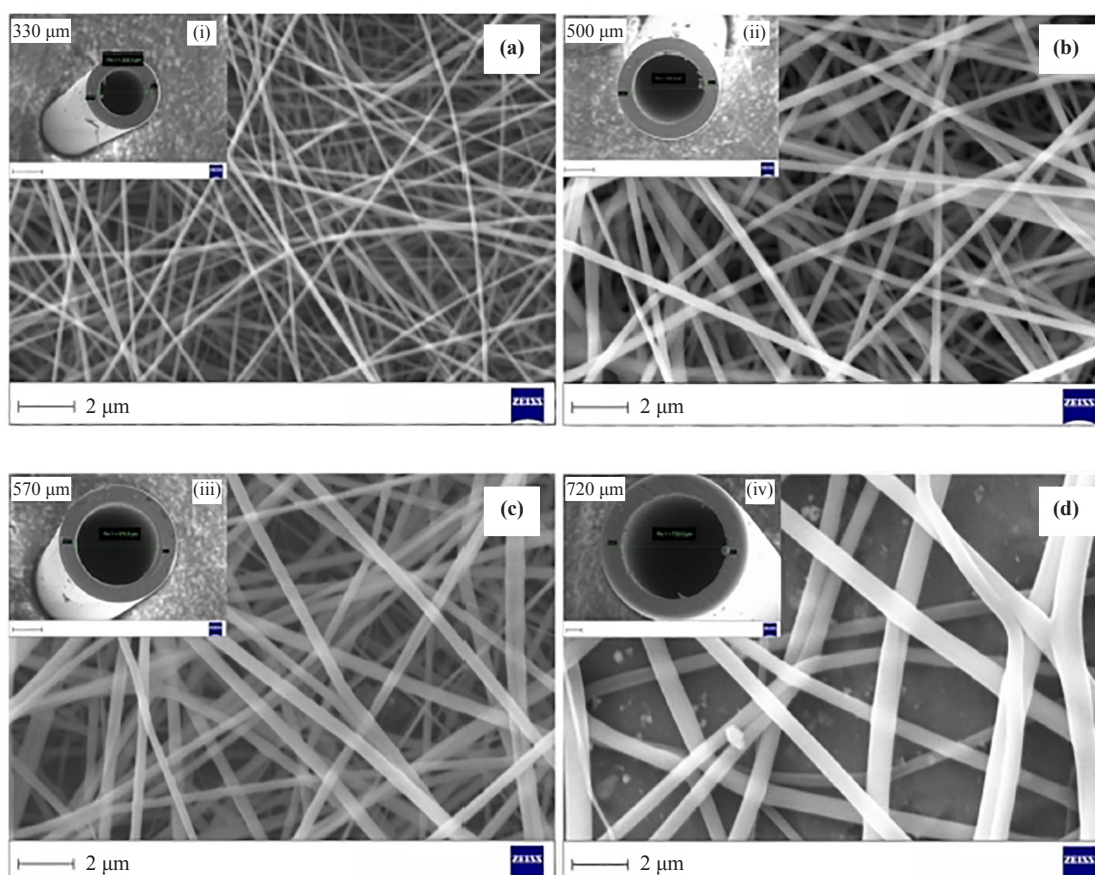


**Figure 13.** SEM images of $TiO_2$ nanofibers spun into different internal needle diameters (a) 330 μm, (b) 500 μm, (c) 570 μm, and (d) 720 μm (insertion: SEM images of the inner diameter of needles). Reprinted with permission from [71]

Another crucial factor in determining the morphology of nanofibers is the pump flow used in electrospinning. That is because a larger volume of solution comes from the needle tip in flows with higher values, causing jets with larger diameters. This higher flow rate means there is no time for the solvent to evaporate, forming thicker nanofibers and, in some cases, granules. However, in lower flow values, there is a smaller droplet formation at the tip of the needle, and consequently, the diameter of the launched jet was smaller. With this, the nanofibers are thinner, and there is a lower remnant of solvent in the nanofibers [66]. In work by Gade and collaborators [74], who studied the different flows (2 mL/h, 5 mL/h, 8 mL/h) of PVDF electrospinning in acetone: DMF (1:1), obtained the following average nanofiber sizes: 218 nm, 248 nm, 308 nm; respectively.

Bakar and collaborators [69] carried out a work addressing the relationship between pump flow and the diameter of the nanofibers. They observed that when working with rates of 10 µL/min, 15 µL/min, and 20 µL/min, they obtained nanofibers of PAN with diameters 512 µm; 444.84 µm; 403.23 µm, respectively.

Another important processing parameter is the diameter of the needle. The effect of this parameter on the morphology of the nanofibers was analyzed using needles with an internal diameter of 330 µm, 500 µm, 570 µm, and 720 µm, employing a PVP-TiO$_2$ solution with 9% mass PVP concentration. Figure 13 shows that the average diameter of TiO$_2$ nanofibers obtained from different needle diameters was $150 \pm 20$ nm, $200 \pm 20$ nm, $250 \pm 20$ nm, and $350 \pm 20$ nm, respectively. The increase in the diameter of the nanofibers with the increase in needle diameter occurs because the Coulomb force decreases the jet's acceleration, and, therefore, the solution moves more slowly [71].

The environmental parameters that determine the morphology and production of nanofibers by electrospinning are temperature and relative humidity (RH). Temperature is directly related to solvent volatility and viscosity of the solution. A work developed by Han and Steckl [58] corroborates a decrease in the diameter of the nanofiber and a decrease in the viscosity of a polyamide-6 solution with the increase in temperature. In addition, there is the finding that the increase in temperature is proportionally related to the evaporation rate of the solvent.

For relative humidity (RH), a correlation between this factor, morphology, and fiber thickness can be established. A work published by Pelipenko[75], which studies the influence of relative humidity on the electrospinning of an aqueous solution of poly(vinyl alcohol) (PVA), found that the diameters of the nanofibers formed decreased from $667 \pm 83$ nm (RH to 4%) to $161 \pm 42$ nm (RH to 60%) with the increase of humidity. With a 70% RH begins to appear the morphology of granule. These results of the morphology of the nanofibers are presented in Figure 14.
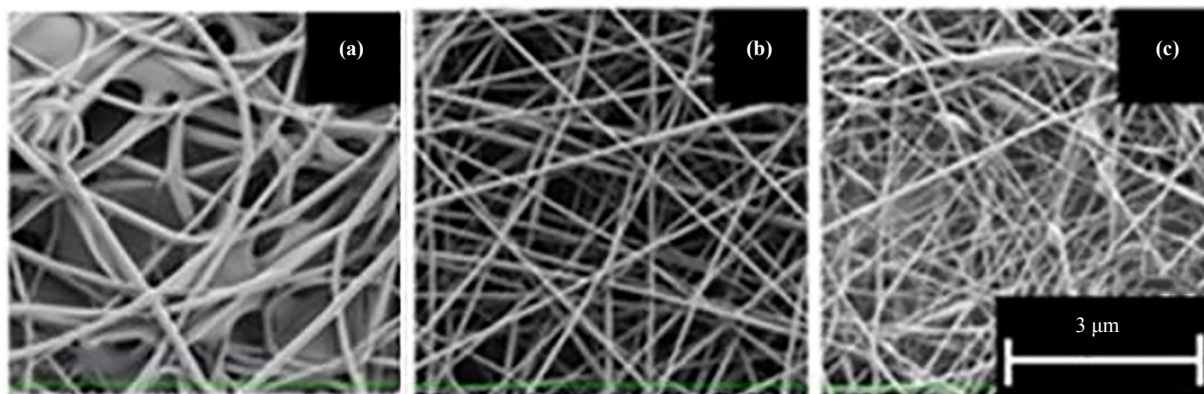


**Figure 14.** SEM images of PVA electrospinning (a) the average fiber diameter is $667 \pm 83$ nm with RH at 4%; (b) $161 \pm 42$ nm with RH to 60%; (c) from $74 \pm 9$ nm with RH at 70%. Reprinted with permission from [75]

The authors explain the appearance of granule morphology by the analogy of the electrospinning jet with the rupture of the capillary fluid, considering the distinction of force responsible for stretching. In the rupture of the capillary fluid, this force is gravitational. In electrospinning, the force responsible is electrostatic due to the applied electric field [75].

Based on this analogy, the authors elaborate a schematic representation shown in Figure 15, reflecting how the

relative humidity increase influences nanofibers' morphology. This increase decelerates the solidification process and allows the liquid to flow longer, forming thinner nanofibers (schematically presented in Figure 15, diagram B). Subsequently, nanofibers gradually form with granule morphology (schematically presented in Figure 15, diagrams C, D). Subsequently, the morphology "beads-on-a-string" occurs due to the instability of the Rayleigh jet [55, 57, 62, 75].

The viscoelastic properties of the polymer solution influence Rayleigh jet formation, jet stability, and nanofiber morphology. Therefore, a balance is needed between elastic (G') and plastic (G) contributions. The elastic component (G') should have its lowest possible value to prevent jet rupture and droplet formation, but it should still be present to allow jet initiation [75-76].

This component increases the jet's tendency to contract, which prevents the start and elongation of the jet and leads to its rupture and droplet formation. On the other hand, sufficient plasticity ensures that the polymer chains in the electrospinning jet do not alter their conformation and remain stretched during the solvent evaporation time [67-68, 76].
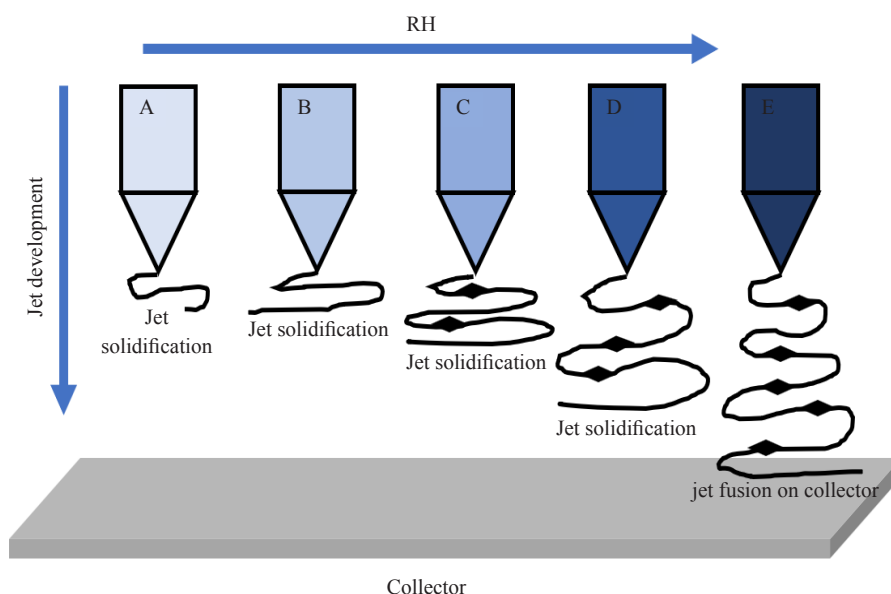


**Figure 15.** Representation of the development of the electrospinning jet under various RH conditions

The authors relate the thickness of the nanofiber with the RH through the evaporation rate of the solvent (water). The volatilization of this solvent is due to the difference between its vapor pressure and its partial pressure in the electrospinning chamber. When the RH is very low, the evaporation rate of the solvent can be so high that it causes a very rapid increase in the local concentration of the polymer and, consequently, a rapid increase in viscosity, which decreases the elongation of the polymer chains that was induced by the applied voltage. However, in RH conditions with higher values, solidification occurs more slowly, and the polymer jet is exposed to stretching for longer, forming thinner fibers [66, 76].

All parameters discussed here, whether those derived from solute, solvent, processing, and/or environmental conditions, will also influence the electrospinning of donor polymers.

## 3.2 Conventional electrospinning applied to donor polymers

The electrospinning of pure P3HT is difficult due to the absence of chain entanglement in the solution. This polymer is in a rigid rod conformation, which would be entanglement, not fulfilling a prerequisite for electrospinning. One of the possibilities for electrospinning P3HT is using a polymer with a very high ability to electrospinning, such as poly(ethylene oxide) (PEO) dissolved in the same P3HT solution. Adding PEO induces chain entanglement, increasing

polymers' viscosity and spinning capacity [77].

However, there are disadvantages in electrospinning P3HT in a polymer mixture, and the first is due to the decrease in conductivity of these fibers compared to pure P3HT. That is because the PEO used in the mixture is considered insulating since the difference between HOMO and LUMO is greater than 3.0 eV [77]. The problem with this methodology for manufacturing nanofibers is obtaining fibers too large to be useful in an OPV device (> 1 μm). In addition, when PCBM is embedded in the solution, there is difficulty in forming nanofibers of the solution containing P3HT:PCBM. That is due to the high miscibility of PCBM in P3HT, which disturbs the tangles of the P3HT chain necessary for fiber formation [78].

In the work of Chan and collaborators [79], it was possible to electrospinning pure P3HT. For this, there was a complete dissolution of P3HT in an appropriate solvent, which was maintained undisturbed for at least 30 min before electrospinning to form continuous fibers. This period allowed sufficient gelling of P3HT, which was described as a two-step process. The first occurred through the formation of rod-like aggregates, followed by a crystallization stage of physical entanglements and cross-links of the aggregates. This physical mechanism of chain-chain entanglement during gelling is necessary for concentrations less than 7% by mass. However, in the work of Lee and collaborators [80], P3HT electrospinning occurred with a concentration of 11%, resulting in large fibers and beaded fibers due to a rapid crystallization of the P3HT.

An example of a conductive polymer that was electrospun was shown in the work published by Fotia et al. [81]. In this, polyaniline was electrospun in solution with two different polymers that have a great ability to electrospun, poly(methyl methacrylate) (PMMA) and poly(vinyl acetate) (PVAc), forming two systems, PANI/PMMA, and PANI/PVAc. The best tissues were obtained in the presence of PVAc, with a conductivity value of two orders of magnitude greater than the system containing PMMA. In addition, the PANI/PVAc sample obtained better capacitive performance. Regardless of the system, the addition of PMMA and PVAc caused a decrease in the electrical conductivity of the tissues.

## 3.3 *Conventional electrospinning applied to BHJ cells*

The first studies with electrospinning to form an active layer of BHJ containing a donor polymer and an acceptor material occurred in the early 2,000s [82]. Liu and collaborators [83] conducted a study with the poly[2,5-bis(20-ethylhexyloxy)-1,4-phenylene vinylene] (BEH-PPV) and the PCBM acceptor material. This study was based on the formation of nanofibers of the donor polymer with different concentrations of methanol. A nanofiber with a uniform diameter of 250 nm and a smooth surface was obtained. Adding PCBM to the polymer solution did not cause major changes in the morphology and diameter of the formed nanofibers. In addition, the absence of granules and aggregates of the acceptor material was observed, even with a ratio of 1:10 between donor polymer and PCBM. This absence of aggregates of the acceptor material can increase percolation pathways, improving the transport of holes and electrons and reducing the occurrences of recombination between these two charge carriers.

Another example was the study conducted by Yang and collaborators [19], whose electrolyte material was poly[2-methoxy-5-(2-ethylhexyloxy)-1,4-phenylenevinylene]/poly(vinyl pyrrolidone)/PCBM (MEH-PPV/PVP/PCBM). Some effects of adding nanofiber were observed, such as increased cell efficiency (by about 20%), diffusion and dissociation of photogenerated excitons in the organic interfaces involved, and greater light absorption. Thus, it was established that electrospinning becomes a method that can be applied to other systems of acceptor-donor materials in the manufacture of solar cell devices to improve the incorporation of nano fibrillar morphologies of polymers conjugated with fullerene compounds.

Another conductive polymer in which the electrospinning process was performed was poly[N-9'-heptadecanyl-2,7-carbazole-alt-5,5-(4',7'-di-2-thienyl-2',1',3'-benzothiadiazole)] (PCDTBT), whose acceptor material was PC$_{70}$BM. In this study, the authors made nanofibers with different diameters (20, 50, 120, and 200 nm) through the viscosity and conductivity control of the solution. The best photovoltaic parameters were obtained using the nanofiber with an average diameter of 20 nm. The OPV device containing these PCDTBT nanofibers showed a short-circuit current density value of 11.54 mA/cm$^2$ and an efficiency of 5.82%. The increased $J_{sc}$ was attributed to improved photon capture and better charge transport. The justification for this fact was that the nanofiber's diameter was approximately twice the diffusion length of the exciton, resulting in the absence of almost 100% of photoluminescence, indicating that the excitons were efficiently dissociated [84-85].

Khanum and Ramamurthy [86] studied three types of active layers for P3HT:PCBM. The first contains only electrospun material (ES), another contains film deposited by the spin-coating (SC) technique, and the third is the junction of the film deposited by spin-coating with nanofibers (ES + SC). It was observed that the efficiency of the device containing only electrospun material was 0.13% due to an irregular interface between the active layer and the cathode, which led to a short circuit of the devices with reduced efficiency. When the active layer containing ES + SC was compared with that deposited only by spin-coating, a considerable increase in efficiency was observed from 2.16% to 3.66%. The reason is that the interface between the donor/acceptor improved. In addition, forming an orderly structure favored a better separation of charges and better transport. This orderly structure resulted in a longer path for light to travel into the active layer, consequently increasing the light absorption performed by the P3HT.

### 3.4 Coaxial electrospinning

This process consists of two nozzles concentrically aligned, and the solutions of the core and shell layers are fed at a controlled rate. Thus, the core solution constitutes the inner layer, and the shell composes the outer layer [86]. Figure 16 represents the coaxial electrospinning process. That starts with applying a voltage that distributes electrical charges on the tip of the needle, causing the shell solution to be attracted and imposing a drag force on the core solution. This drag causes the formation of Taylor's cone, from which a jet is ejected and subsequently undergoes stretching and formation of the nanofibers. There are two obligations for coaxial electrospinning: the shell layer must be able to electrospinning, and the interfacial tension between the core-shell layers should be the lowest possible (2).
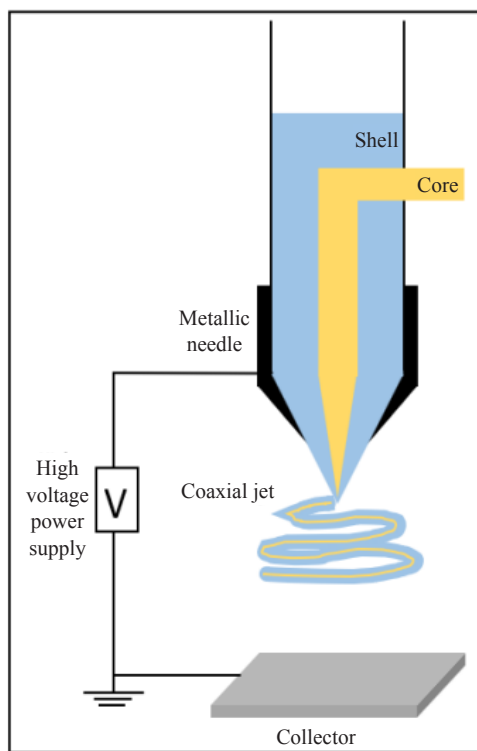


**Figure 16.** Coaxial electrospinning equipment

### 3.5 Coaxial electrospinning applied to BHJ

Coaxial electrospinning can electrospun a solution containing the donor polymer and the acceptor material as a

core layer. Sundarrajan and collaborators [87] performed coaxial electrospinning of P3HT:PCBM as a core layer and polyvinylpyrrolidone (PVP) being the shell layer. The shell layer was removed by washing with ethanol, which caused a decrease of 0.94 μm in the diameter of the fibers. When comparing the electrospun tissue with the film obtained by spin coating of P3HT:PCBM, a decrease in the optical bandgap of the P3HT was observed in a value of 0.03 eV. In addition, the absorption band was displaced to the wavelength region in red. This displacement was related to the fact that the nanofibers induced the relocation of the π conjugation in the polymer chains due to the elongation of the chains during the electrospinning process. In this study, the researchers obtained a device efficiency of only $8.7 \times 10^{-8}$ due to the processing of the tissue composed of nanofiber that occurred under inapt environmental conditions (electrospinning and washing with ethanol). In addition, the thickness of the tissue containing nanofiber was approximately 5 μm, and the diffusion length of the charge carriers in organic solar cells is only a few nanometers. Therefore, most charge carriers were lost in the fiber matrix [87].

Bedford and collaborators [78] produced P3HT:PCBM fibers through coaxial electrospinning using polycaprolactone (PCL) as a sacrifice layer. The average size of the nanofibers obtained was $120 \pm 30$ nm after removing the shell layer with cyclopentanone. The devices containing the nanofiber in the active layer showed a PCE value of 4.0%, while the devices with only thin films showed a PCE value of 3.2%. The addition of nanofibers increased other parameters of the photovoltaic cell, such as the JSC and the fill factor (FF). That was due to the increased alignment of P3ht polymer chains in the nanoscale caused by electrospinning, which led to increased optical absorption and subsequent generation of the exciton.

In the study by Huang and collaborators [49], P3HT:PC$_{61}$BM fibers were obtained by coaxial electrospinning using polyethylene glycol (PEG) as a shell layer. The addition of cyclopentanone performed the subsequent removal of the shell layer. The fibers obtained presented a diameter of 150-160 nm and were incorporated into a film of P3HT:PC$_{61}$BM to make up the device's active layer. The authors compared the device containing the nanofibers with the one prepared in their absence. The efficiency of the solar cell increased by 62% in the presence of nanofibers due to greater interaction between the P3HT chains and greater absorption of photons caused by the increase in the π-π* transition along the oriented fibers.

**Table 1.** PCE of devices with nanofibers.

| Shell-Core | Donor: Acceptor | PCE without nanofiber (%) | PCE with Nanofiber (%) | Ref. |
|---|---|---|---|---|
| PVP-P3HT:PCBM | P3HT:PCBM | - | $8.7 \times 10^{-8}$ | [87] |
| PCL-P3HT:PCBM | P3HT:PCBM | 3.2 | 4.0 | [78] |
| PEG-P3HT:PC$_{61}$BM | P3HT:PC$_{61}$BM | 2.98 | 4.84 | [49] |

In the work of Kim and collaborators [88], the coaxial electrospinning of the P3HT:PCBM was performed with the PVP shell layer. The authors discussed the structural results of fiber formation through X-ray diffraction (XRD) analysis, relating the shear and Coulomb forces present in the electrospinning process. They found that these forces influence the orientation of the polymer chain synergistically, in which the shear force arises as the fiber flows through the needle at a very high rate. The Coulomb force is through the applied electric field, which lengthens the polymer chains.

Another way to obtain the active layer through electrospinning was shown in the study by Pierini and collaborators [89], in which there is the use of single-material organic solar cells (SMOCs), highly efficient, based on polythiophenes grafted with fullerene and the shell layer was PEO. The chains of the donor polymer were chemically designed, allowing high solubility, molar mass, and regioregularity. In addition, the authors established a correlation between the hierarchical structure of the active layer given by incorporating electrospun nanofibers and the photovoltaic properties of the solar cell. The efficiency of SMOCs can be strongly increased with the optimization of the supramolecular structure and nanoscale of the active layer, reaching the highest efficiency value of 5.58%. In general, the work demonstrated that the structural optimization of the active material obtained by including electrospun nanofibers promoted the

development of copolymer crystalline due to π-π stacking between chains. In addition, these features contributed to greater efficiency of UV-Vis radiation absorption, the creation of paths for charge carriers, and the improvement of mechanical properties.

Another application for coaxial electrospinning is in the manufacture of ternary organic cells. These have at least three components, one of which is an electron acceptor material and two electron donor materials. The two conductive polymers used had the characteristic of having the complementary absorption spectrum so that there was a better use for absorption of the solar spectrum and, consequently, a greater generation of photons. The additional component can help improve charge transport and/or decrease charge recombination issues associated with binary devices. It can also increase charge mobility and decrease the density of trap states, allowing ternary cells to have an improved FF and thick active layers (greater than 200 nm) [16].

Huang and collaborators [49] carried out a work that exemplifies coaxial electrospinning in a ternary organic solar cell. These researchers developed a device in which the active layer had nanofibers from coaxial electrospinning, whose shell layer was PEG. The active layer comprised P3HT/PTB7:$PC_{61}BM$. The PTB7 polymer was chosen due to the possibility of compensating for the weak absorption of P3HT in the wavelength range of 650-750 nm, causing the system to capture a larger region of the solar spectrum. The system's efficiency increased by 26% with the addition of nanofibers. Another cell parameter that increased was $J_{sc}$, indicating a higher absorption of photons, higher charge generation, decreased recombination, and greater mobility of charges.

Jin et al. [90] proposed building a conductive polymer's core-shell morphology using a differentiated experimental form. The polymer used was poly(3,4-ethylene dioxythiophene) (PEDOT), one of the polythiophene derivatives. Its employability is related to its excellent environmental and thermal stability, good mechanical properties, low redox potential, and high optical transparency. It can be used as a hole transport layer (HTL). The authors performed the electrospinning of poly(vinyl chloride) (PVC) using different flows (0.5 mL.h$^{-1}$, 1.5 mL.h$^{-1}$, and 3.0 mL.h$^{-1}$). Subsequently, PEDOT was coated on the surface of PVC nanofibers employing rapid interfacial in situ polymerization using iron chloride as an oxidant. The shell layer was the PEDOT, and the core layer was the PVC. The polymerization occurred at 20, 40, and 60 °C. The average diameters of the PVC nanofibers obtained were 310 nm (PVC-310), 650 nm (PVC-650), and 1,100 nm (PVC-1,100), corresponding to feed rates of 0,5 mL.h$^{-1}$; 1,5 mL.h$^{-1}$ e 3,0 mL.h$^{-1}$. The material's conductivity was measured by cyclic voltammetry and electrochemical impedance spectroscopy. Cyclic voltammetry showed that the PEDOT-650 sample presented the highest charge storage capacity compared to the other SAMPLES of PEDOT-310 and PEDOT-1,100. The conductivity of the nanofibers of PEDOT-650 was 7.8 S.cm$^{-1}$, while the conductivities of PEDOT-310 and PEDOT-1,100 were 5.3 S.cm$^{-1}$ and 4.3 S.cm$^{-1}$, respectively. This result is due to the difference in the tissues' porosity and the PEDOT layer's thickness caused by the change in the diameter of PVC nanofibers. The reaction's temperature affected the nanofibers' conductivity because, at the lowest temperature, there was a slower solvent evaporation, which caused a higher crystallinity.

**Table 2.** PCE of photovoltaic devices from donor and acceptor materials

| Donor | Acceptor | PCE (%) | Ref. |
| --- | --- | --- | --- |
| PM6 | BTP-4Cl | 16.50 | 91 |
| PM6 | BTP-4Cl-12 | 17.00 | 92 |
| D18 | Y6 | 18.22 | 93 |
| PTQ10 | Y6 | 16.21 | 94 |

There is still a great need to increase the photovoltaic parameters of BHJ organic solar cells, either by modifying and improving the materials involved in the active layer or changing the layer's morphology. The electrospinning process is a very important tool, with low cost, relative speed, and efficiency, for the insertion of nanofibers to promote

structural changes and consequently increase the efficiency of these devices. It should also be noted that electrospinning can produce nanofibers from any electron donor-acceptor pair, extending its use to developing new materials. The work perspective would be to use this method of coaxial electrospinning for OPVs containing non-fullerene acceptors whose efficiencies of these solar cells are close to 20%. The possibilities of the donor polymer and the acceptor material are presented in Table 2.

## 4. Summary

There is still a great need to increase the photovoltaic parameters of BHJ organic solar cells, either by modifying and improving the materials involved in the active layer or by changing the morphology of this layer. The electrospinning process is a very important tool, with low cost, relative speed and efficiency, for the insertion of nanofibers of the components of the active layer to promote structural changes and consequently increase the efficiency of these devices. It should also be noted that electrospinning can produce nanofibers of any electron donor-acceptor pair, extending its use to developing new photovoltaic devices employing the most efficient organic semiconductors developed today.

## Conflict of interest

The authors declare no competing financial interest. They have no known competing financial interests or personal relationships that could have appeared to influence the work reported in this paper.

## References

[1] Elheddad M, Benjasak C, Deljavan R, Alharthi M, Almabrok JM. The effect of the Fourth Industrial Revolution on the environment: The relationship between electronic finance and pollution in OECD countries. *Technological Forecasting and Social Change*. 2021; 163: 120485.

[2] Wang M, Wang K, Yang Y, Liu Y, Yu DG. Electrospun environment remediation nanofibers using unspinnable liquids as the sheath fluids: A review. *Polymers*. 2020; 12(1): 103.

[3] Ye L, Jiao X, Zhou M, Zhang S, Yao H, Zhao W, et al. Manipulating aggregation and molecular orientation in all-polymer photovoltaic cells. *Advanced Materials*. 2015; 27(39): 6046-6054.

[4] Gong M, Zhang L, Wan P. Polymer nanocomposite meshes for flexible electronic devices. *Progress in Polymer Science*. 2020; 107: 101279.

[5] Ajayan J, Nirmal D, Mohankumar P, Saravanan M, Jagadesh M, Arivazhagan L. A review of photovoltaic performance of organic/inorganic solar cells for future renewable and sustainable energy technologies. *Superlattices and Microstructures*. 2020; 143: 106549.

[6] Ikpesu JE, Iyuke SE, Daramola M, Okewale AO. Synthesis of improved dye-sensitized solar cell for renewable energy power generation. *Solar Energy*. 2020; 206: 918-934.

[7] Xiao J, Yan T, Lei T, Li Y, Han Y, Song W, et al. Organic solar cells based on non-fullerene acceptors of nine fused-ring by modifying end groups. *Organic Electronics*. 2020; 81: 105662.

[8] Rafique S, Abdullah SM, Sulaiman K, Iwamoto M. Fundamentals of bulk heterojunction organic solar cells: An overview of stability/degradation issues and strategies for improvement. *Renewable and Sustainable Energy Reviews*. 2018; 84: 43-53.

[9] Karuthedath S, Gorenflot J, Firdaus Y, Chaturvedi N, De Castro CS, Harrison GT, et al. Intrinsic efficiency limits in low-bandgap non-fullerene acceptor organic solar cells. *Nature Materials*. 2021; 20(3): 378-384.

[10] Sun R, Guo J, Sun C, Wang T, Luo Z, Zhang Z, et al. A universal layer-by-layer solution-processing approach for efficient non-fullerene organic solar cells. *Energy & Environmental Science*. 2019; 12(1): 384-395.

[11] Elumalai NK, Uddin A. Open circuit voltage of organic solar cells: An in-depth review. *Energy & Environmental Science*. 2016; 9(2): 391-410.

[12] Park JS, Kim GU, Lee D, Lee S, Ma B, Cho S, et al. Importance of optimal crystallinity and hole mobility of BDT-based polymer donor for simultaneous enhancements of $V_{oc}$, $J_{sc}$, and FF in efficient nonfullerene organic solar cells.

*Advanced Functional Materials*. 2020; 30(51): 2005787.

[13] Park SH, Park S, Kurniawan D, Son JG, Noh JH, Ahn H, et al. Highly efficient large-area organic photovoltaic module with a 350 nm thick active layer using a random terpolymer donor. *Chemistry of Materials*. 2020; 32(8): 3469-3479.

[14] Bartesaghi D, Pérez ID, Kniepert J, Roland S, Turbiez M, Neher D, et al. Competition between recombination and extraction of free charges determines the fill factor of organic solar cells. *Nature Communications*. 2015; 6(1): 7083.

[15] Yang C, Zhang S, Ren J, Gao M, Bi P, Ye L, et al. Molecular design of a non-fullerene acceptor enables a P3HT-based organic solar cell with 9.46% efficiency. *Energy & Environmental Science*. 2020; 13(9): 2864-2869.

[16] Zhang KN, Jiang ZN, Wang T, Qiao JW, Feng L, Qin CC, et al. Exploring the mechanisms of exciton diffusion improvement in ternary polymer solar cells: From ultrafast to ultraslow temporal scale. *Nano Energy.* 2021; 79: 105513.

[17] Muchuweni E, Martincigh BS, Nyamori VO. Organic solar cells: Current perspectives on graphene-based materials for electrodes, electron acceptors and interfacial layers. *International Journal of Energy Research*. 2021; 45(5): 6518-6549.

[18] Yan H, Tang Y, Sui X, Liu Y, Gao B, Liu X, et al. Increasing quantum efficiency of polymer solar cells with efficient exciton splitting and long carrier lifetime by molecular doping at heterojunctions. *ACS Energy Letters*. 2019; 4(6): 1356-1363.

[19] Wang Y, Luke J, Privitera A, Rolland N, Labanti C, Londi G, et al. The critical role of the donor polymer in the stability of high-performance non-fullerene acceptor organic solar cells. *Joule*. 2023; 7(4): 810-829.

[20] Yu G, Gao J, Hummelen JC, Wudl F, Heeger AJ. Polymer photovoltaic cells: enhanced efficiencies via a network of internal donor-acceptor heterojunctions. *Science*. 1995; 270(5243): 1789-1791.

[21] Kim T, Im JH, Choi HS, Yang SJ, Kim SW, Park CR. Preparation and photoluminescence (PL) performance of a nanoweb of P3HT nanofibers with diameters below 100 nm. *Journal of Materials Chemistry*. 2011; 21(37): 14231-14239.

[22] Wu J, Xu Y, Yang Z, Chen Y, Sui X, Yang L, et al. Simultaneous enhancement of three parameters of P3HT-based organic solar cells with one oxygen atom. *Advanced Energy Materials*. 2019; 9(6): 1803012.

[23] Shaban M, Benghanem M, Almohammedi A, Rabia M. Optimization of the active layer P3HT: PCBM for organic solar cell. *Coatings*. 2021; 11(7): 863.

[24] Liao SH, Jhuo HJ, Cheng YS, Chen SA. Fullerene derivative-doped zinc oxide nanofilm as the cathode of inverted polymer solar cells with low-bandgap polymer (PTB7-Th) for high performance. *Advanced Materials*. 2013; 25(34): 4766-4771.

[25] Wan Q, Guo X, Wang Z, Li W, Guo B, Ma W, et al. 10.8% efficiency polymer solar cells based on PTB7-Th and $PC_{71}BM$ via binary solvent additives treatment. *Advanced Functional Materials*. 2016; 26(36): 6635-6640.

[26] Yu G, Gao J, Hummelen JC, Wudl F, Heeger AJ. Polymer photovoltaic cells: Enhanced efficiencies via a network of internal donor-acceptor heterojunctions. *Science*. 1995; 270(5243): 1789-1791.

[27] Li Y. Molecular design of photovoltaic materials for polymer solar cells: Toward suitable electronic energy levels and broad absorption. *Accounts of Chemical Research*. 2012; 45(5): 723-733.

[28] Zhao W, Qian D, Zhang S, Li S, Inganäs O, Gao F, et al. Fullerene-free polymer solar cells with over 11% efficiency and excellent thermal stability. *Advanced Materials*. 2016; 28(23): 4734-4739.

[29] Chen Y, Wan X, Long G. High performance photovoltaic applications using solution-processed small molecules. *Accounts of Chemical Research*. 2013; 46(11): 2645-2655.

[30] Li M, Gao K, Wan X, Zhang Q, Kan B, Xia R, et al. Solution-processed organic tandem solar cells with power conversion efficiencies > 12%. *Nature Photonics*. 2017; 11(2): 85-90.

[31] Liu J, Chen S, Qian D, Gautam B, Yang G, Zhao J, et al. Fast charge separation in a non-fullerene organic solar cell with a small driving force. *Nature Energy*. 2016; 1(7): 1-7.

[32] Ye L, Jiao X, Zhou M, Zhang S, Yao H, Zhao W, et al. Manipulating aggregation and molecular orientation in all-polymer photovoltaic cells. *Advanced Materials*. 2015; 27(39): 6046-6054.

[33] Jung JW, Jo JW, Chueh CC, Liu F, Jo WH, Russell TP, et al. Fluoro-substituted n-type conjugated polymers for additive-free all-polymer bulk heterojunction solar cells with high power conversion efficiency of 6.71%. *Advanced Materials*. 2015; 27(21): 3310-3317.

[34] Lee J, Singh R, Sin DH, Kim HG, Song KC, Cho K. A nonfullerene small molecule acceptor with 3D interlocking geometry enabling efficient organic solar cells. *Advanced Materials*. 2016; 28(1): 69-76.

[35] Halls JJ, Walsh CA, Greenham NC, Marseglia EA, Friend RH, Moratti SC, et al. Efficient photodiodes from interpenetrating polymer networks. *Nature*. 1995; 376(6540): 498-500.

[36] Zhao W, Li S, Yao H, Zhang S, Zhang Y, Yang B, et al. Molecular optimization enables over 13% efficiency in organic solar cells. *Journal of the American Chemical Society*. 2017; 139(21): 7148-7151.

[37] Li S, Ye L, Zhao W, Zhang S, Mukherjee S, Ade H, et al. Energy-level modulation of small-molecule electron acceptors to achieve over 12% efficiency in polymer solar cells. *Advanced Materials*. 2016; 28(42): 9423-9429.

[38] Li H, Earmme T, Ren G, Saeki A, Yoshikawa S, Murari NM, et al. Beyond fullerenes: Design of nonfullerene acceptors for efficient organic photovoltaics. *Journal of the American Chemical Society*. 2014; 136(41): 14589-14597.

[39] Guo X, Facchetti A, Marks TJ. Imide-and amide-functionalized polymer semiconductors. *Chemical Reviews*. 2014; 114(18): 8943-9021.

[40] Shin WS, Jeong HH, Kim MK, Jin SH, Kim MR, Lee JK, et al. Effects of functional groups at perylene diimide derivatives on organic photovoltaic device application. *Journal of Materials Chemistry*. 2006; 16(4): 384-390.

[41] Long X, Ding Z, Dou C, Zhang J, Liu J, Wang L. Polymer acceptor based on double B ← N bridged bipyridine (BNBP) unit for high-efficiency all-polymer solar cells. *Advanced Materials*. 2016; 28(30): 6504-6508.

[42] Zhan X, Tan ZA, Domercq B, An Z, Zhang X, Barlow S, et al. A high-mobility electron-transport polymer with broad absorption and its use in field-effect transistors and all-polymer solar cells. *Journal of the American Chemical Society*. 2007; 129(23): 7246-7247.

[43] Zhou Y, Kurosawa T, Ma W, Guo Y, Fang L, Vandewal K, et al. High performance all-polymer solar cell via polymer side-chain engineering. *Advanced Materials*. 2014; 26(22): 3767-3772.

[44] Guo Y, Li Y, Awartani O, Zhao J, Han H, Ade H, et al. A vinylene-bridged perylenediimide-based polymeric acceptor enabling efficient all-polymer solar cells processed under ambient conditions. *Advanced Materials*. 2016; 28(38): 8483-8489.

[45] Ben Dkhil S, Pfannmöller M, Schröder RR, Alkarsifi R, Gaceur M, Köntges W, et al. Interplay of interfacial layers and blend composition to reduce thermal degradation of polymer solar cells at high temperature. *ACS Applied Materials & Interfaces*. 2018; 10(4): 3874-3884.

[46] Vithanage DA, Matheson AB, Pranculis V, Hedley GJ, Pearson SJ, Gulbinas V, et al. Barrierless slow dissociation of photogenerated charge pairs in high-performance polymer-fullerene solar cells. *The Journal of Physical Chemistry C*. 2017; 121(26): 14060-14065.

[47] Manley EF, Strzalka J, Fauvell TJ, Jackson NE, Leonardi MJ, Eastham ND, et al. In situ GIWAXS analysis of solvent and additive effects on PTB7 thin film microstructure evolution during spin coating. *Advanced Materials*. 2017; 29(43): 1703933.

[48] Kaltenbrunner M, White MS, Głowacki ED, Sekitani T, Someya T, Sariciftci NS, et al. Ultrathin and lightweight organic solar cells with high flexibility. *Nature Communications*. 2012; 3(1): 770.

[49] Huang HJ, Nan HR, Yang YG, Gao XY, Chen F, Chen ZK. Improved performance of thick films based binary and ternary bulk heterojunction organic photovoltaic devices incorporated with electrospinning processed nanofibers. *Advanced Materials Interfaces*. 2018; 5(20): 1800914.

[50] Kim YJ, An TK, Park CE. Morphological studies of small-molecule solar cells: nanostructural engineering via solvent vapor annealing treatments. *Journal of Materials Science*. 2017; 52(22): 13173-13182.

[51] Bhardwaj N, Kundu SC. Electrospinning: A fascinating fiber fabrication technique. *Biotechnology Advances*. 2010; 28(3): 325-347.

[52] Han J, Xiong L, Jiang X, Yuan X, Zhao Y, Yang D. Bio-functional electrospun nanomaterials: From topology design to biological applications. *Progress in Polymer Science*. 2019; 91: 1-28.

[53] Ghorani B, Tucker N. Fundamentals of electrospinning as a novel delivery vehicle for bioactive compounds in food nanotechnology. *Food Hydrocolloids*. 2015; 51: 227-240.

[54] Barhoum A, Pal K, Rahier H, Uludag H, Kim IS, Bechelany M. Nanofibers as new-generation materials: From spinning and nano-spinning fabrication techniques to emerging applications. *Applied Materials Today*. 2019; 17: 1-35.

[55] Liu M, Deng N, Ju J, Fan L, Wang L, Li Z, et al. A review: Electrospun nanofiber materials for lithium-sulfur batteries. *Advanced Functional Materials*. 2019; 29(49): 1905467.

[56] Zhang X, Xie L, Wang X, Shao Z, Kong B. Electrospinning super-assembly of ultrathin fibers from single-to multi-Taylor cone sites. *Applied Materials Today*. 2022; 26: 101272.

[57] Guo H, Chen Y, Li Y, Zhou W, Xu W, Pang L, et al. Electrospun fibrous materials and their applications for electromagnetic interference shielding: A review. *Composites Part A: Applied Science and Manufacturing*. 2021; 143: 106309.

[58] Han D, Steckl AJ. Coaxial electrospinning formation of complex polymer fibers and their applications. *ChemPlusChem*. 2019; 84(10): 1453-1497.

[59] Liu F, Vyas C, Yang J, Ates G, Bártolo PJ. A review of hybrid biomanufacturing systems applied in tissue regeneration. In: Bidanda B, Bártolo PJ. (eds.) *Virtual Prototyping & Bio Manufacturing in Medical Applications*. Springer, Cham; 2021. p.187-213.

[60] Rwei SP, Huang CC. Electrospinning PVA solution-rheology and morphology analyses. *Fibers and Polymers*. 2012; 13: 44-50.

[61] Xue J, Wu T, Dai Y, Xia Y. Electrospinning and electrospun nanofibers: Methods, materials, and applications. *Chemical Reviews*. 2019; 119(8): 5298-5415.

[62] Kang S, Zhao K, Yu DG, Zheng X, Huang C. Advances in biosensing and environmental monitoring based on electrospun nanofibers. *Advanced Fiber Materials*. 2022; 4(3): 404-435.

[63] Levitt AS, Vallett R, Dion G, Schauer CL. Effect of electrospinning processing variables on polyacrylonitrile nanoyarns. *Journal of Applied Polymer Science*. 2018; 135(25): 46404.

[64] Li J, Liu Y, Abdelhakim HE. Drug delivery applications of coaxial electrospun nanofibres in cancer therapy. *Molecules*. 2022; 27(6): 1803.

[65] Joshi B, Samuel E, Kim YI, Yarin AL, Swihart MT, Yoon SS. Review of recent progress in electrospinning-derived freestanding and binder-free electrodes for supercapacitors. *Coordination Chemistry Reviews*. 2022; 460: 214466.

[66] Guo Q, Zhang X. A review of mechanochromic polymers and composites: From material design strategy to advanced electronics application. *Composites Part B: Engineering*. 2021; 227: 109434.

[67] Bavatharani C, Muthusankar E, Wabaidur SM, Alothman ZA, Alsheetan KM, Mana AL-Anazy M, et al. Electrospinning technique for production of polyaniline nanocomposites/nanofibres for multi-functional applications: A review. *Synthetic Metals*. 2021; 1(271): 116609.

[68] Bagherzadeh R, Gorji M, Bafgi MS, Saveh-Shemshaki N. Electrospun conductive nanofibers for electronics. *Electrospun Nanofibers: Woodhead Publishing Series in Textiles*. 2017; 467-519. Available from: https://doi.org/10.1016/B978-0-08-100907-9.00018-0.

[69] Bakar SS, Fong KC, Eleyas A, Nazeri MF. Effect of voltage and flow rate electrospinning parameters on polyacrylonitrile electrospun fibers. *InIOP Conference Series: Materials Science and Engineering*. 2018; 318: 012076.

[70] Al-Dhahebi AM, Saheed MS, Mustapha M. Effects of solution concentration on the synthesis of polyvinylidene fluoride (PVDF) electrospun nanofibers. *Materials Today: Proceedings*. 2023; 80: 2119-2124.

[71] Kuchi C, Harish GS, Reddy PS. Effect of polymer concentration, needle diameter and annealing temperature on $TiO_2$-PVP composite nanofibers synthesized by electrospinning technique. *Ceramics International*. 2018; 44(5): 5266-5272.

[72] Lee H, Jiang Z, Yokota T, Fukuda K, Park S, Someya T. Stretchable organic optoelectronic devices: Design of materials, structures, and applications. *Materials Science and Engineering: R: Reports*. 2021; 146: 100631.

[73] Wang Y, Nie H, Han J, An Y, Zhang YM, Zhang SX. Green revolution in electronic displays expected to ease energy and health crises. *Light: Science & Applications*. 2021; 10(1): 33.

[74] Gade H, Nikam S, Chase GG, Reneker DH. Effect of electrospinning conditions on β-phase and surface charge potential of PVDF fibers. *Polymer*. 2021; 228: 123902.

[75] Pelipenko J, Kristl J, Janković B, Baumgartner S, Kocbek P. The impact of relative humidity during electrospinning on the morphology and mechanical properties of nanofibers. *International Journal of Pharmaceutics*. 2013; 456(1): 125-134.

[76] Wang Y, Nie H, Han J, An Y, Zhang YM, Zhang SX. Green revolution in electronic displays expected to ease energy and health crises. *Light: Science & Applications*. 2021; 10(1): 33.

[77] Dillard C, Singhal R, Kalra V. Hierarchical self-assembly in monoaxially electrospun P3HT/PCBM nanofibers. *Macromolecular Materials and Engineering*. 2015; 300(3): 320-327.

[78] Bedford NM, Dickerson MB, Drummy LF, Koerner H, Singh KM, Vasudev MC, et al. Nanofiber-based bulk-heterojunction organic solar cells using coaxial electrospinning. *Advanced Energy Materials*. 2012; 2(9): 1136-1144.

[79] Chan KH, Yamao T, Kotaki M, Hotta S. Unique structural features and electrical properties of electrospun conjugated polymer poly (3-hexylthiophene)(P3HT) fibers. *Synthetic Metals*. 2010; 160(23-24): 2587-2595.

[80] Lee S, Moon GD, Jeong U. Continuous production of uniform poly (3-hexylthiophene)(P3HT) nanofibers by electrospinning and their electrical properties. *Journal of Materials Chemistry*. 2009; 19(6): 743-748.

[81] Fotia A, Malara A, Paone E, Bonaccorsi L, Frontera P, Serrano G, et al. Self standing mats of blended polyaniline produced by electrospinning. *Nanomaterials*. 2021; 11(5): 1269.

[82] Joly D, Jung JW, Kim ID, Demadrille R. Electrospun materials for solar energy conversion: Innovations and trends. *Journal of Materials Chemistry C*. 2016; 4(43): 10173-10197.

[83] Liu HA, Zepeda D, Ferraris JP, Balkus Jr KJ. Electrospinning of poly (alkoxyphenylenevinylene) and methanofullerene nanofiber blends. *ACS Applied Materials & Interfaces*. 2009; 1(9): 1958-1965.

[84] Kim T, Yang SJ, Kim SK, Choi HS, Park CR. Preparation of PCDTBT nanofibers with a diameter of 20 nm and their application to air-processed organic solar cells. *Nanoscale*. 2014; 6(5): 2847-2854.

[85] Khanum KK, Ramamurthy PC. Instigating network structure in bulk heterojunction organic solar cells creating a unique approach in augmenting the optical absorption. *Polymer*. 2016; 91: 146-155.

[86] Chen JY, Chiu YC, Shih CC, Wu WC, Chen WC. Electrospun nanofibers with dual plasmonic-enhanced luminescent solar concentrator effects for high-performance organic photovoltaic cells. *Journal of Materials Chemistry A*. 2015; 3(29): 15039-15048.

[87] Sundarrajan S, Murugan R, Nair AS, Ramakrishna S. Fabrication of P3HT/PCBM solar cloth by electrospinning technique. *Materials Letters*. 2010; 64(21): 2369-2372.

[88] Kim M, Jo SB, Park JH, Cho K. Flexible lateral organic solar cells with core-shell structured organic nanofibers. *Nano Energy*. 2015; 18: 97-108.

[89] Pierini F, Lanzi M, Nakielski P, Pawłowska S, Urbanek O, Zembrzycki K, et al. Single-material organic solar cells based on electrospun fullerene-grafted polythiophene nanofibers. *Macromolecules*. 2017; 50(13): 4972-4981.

[90] Jin L, Wang T, Feng ZQ, Leach MK, Wu J, Mo S, et al. A facile approach for the fabrication of core-shell PEDOT nanofiber mats with superior mechanical properties and biocompatibility. *Journal of Materials Chemistry B*. 2013; 1(13): 1818-1825.

[91] Cui Y, Yao H, Zhang J, Zhang T, Wang Y, Hong L, et al. Over 16% efficiency organic photovoltaic cells enabled by a chlorinated acceptor with increased open-circuit voltages. *Nature Communications*. 2019; 10(1): 2515-2523.

[92] Cui Y, Yao H, Hong L, Zhang T, Tang Y, Lin B, et al. 17% efficiency organic photovoltaic cell with superior processability. *National Science Review*. 2019; 7(7): 1239-1246.

[93] Liu Q, Jiang Y, Jin K, Qin J, Xu J, Li W, et al. 18% Efficiency organic solar cells. *Science Bulletin*. 2020; 65: 272-275.

[94] Sun C, Pan F, Chen S, Wang R, Sun R, Shang Z, et al. Achieving fast charge separation and low nonradiative recombination loss by rational fluorination for high-efficiency polymer solar cells. *Advanced Materials*. 2019; 31: 1905480.